Title

FAULTS AND GRAVITY ANOMALIES OVER THE EAST MESA HYDR0THERMAI-GEOTHERMAL SYSTEM

Authors

Goldstein, N.E.
Carle, S.

Publication Date

1986-05-01

Lawrence Berkeley Laboratory
UNIVERSITY OF CALIFORNIA

EARTH SCIENCES DIVISION

To be presented at the 1986 Annual Meeting of the Geothermal Resources Council, Palm Springs, CA, September 29 - October 1, 1986

FAULTS AND GRAVITY ANOMALIES OVER THE EAST MESA HYDROTHERMAL-GEOTHERMAL SYSTEM

N.E. Goldstein and S. Carle

May 1986

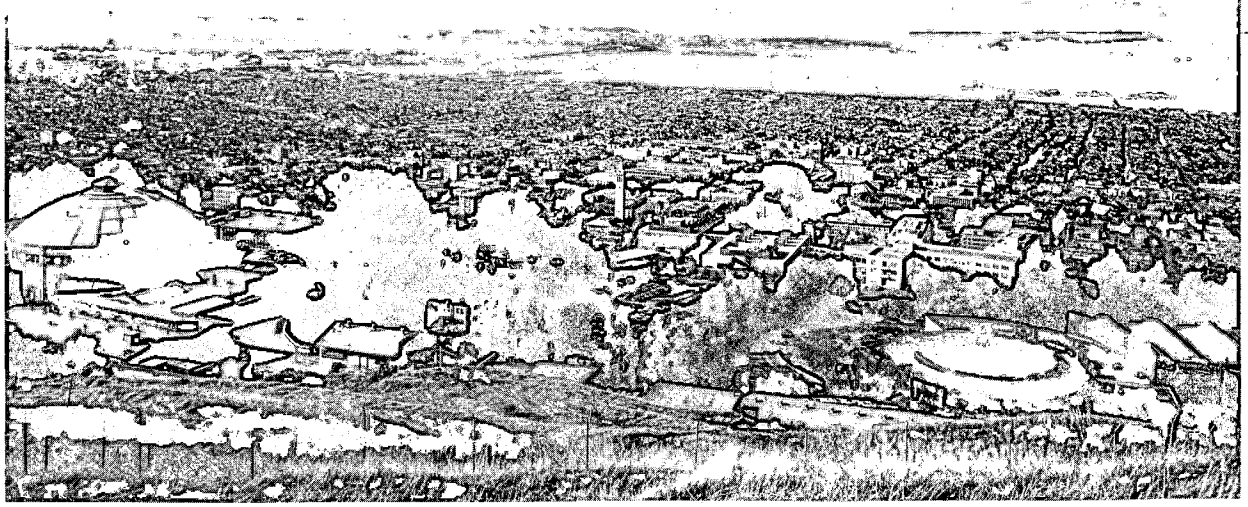

Prepared for the U.S. Department of Energy under Contract DE-AC03-76SF00098

DISCLAIMER

LBL-21459

FAULTS AND GRAVITY ANOMALIES OVER THE EAST MESA HYDROTHERMAL-GEOTHERMAL SYSTEM

N.E. Goldstein and S. Carle

Earth Sciences Division
Lawrence Berkeley Laboratory
University of California
Berkeley, California 94720

May 1986

This work was supported by the Assistant Secretary for Conservation and Renewable Technology, Office of Renewable Energy Technologies, Division of Geothermal Technology of the U.S. Department of Energy under Contract No. DE-AC03-76SF00098.

FAULTS AND GRAVITY ANOMALIES OVER THE EAST MESA HYDROTHERMAL-GEOTHERMAL SYSTEM

N. E. Goldstein and S. Carle

Earth Sciences Division, Lawrence Berkeley Laboratory
University of California, Berkeley, CA 94720

Abstract

Detailed interpretations of gravity anomalies over geothermal systems may be extremely useful for mapping the fracture or fault systems that control the circulation of the thermal waters. This approach seems to be particularly applicable in areas like the Salton Trough where reactions between the thermal waters and the porous sediments produce authigenic-hydrothermal minerals in sufficient quantity to cause distinct gravity anomalies at the surface. A 3-D inversion of the residual Bouguer gravity anomaly over the East Mesa geothermal field was made to examine the densified volume of rock. We show that the data not only resolve a north-south and an intersecting northwest structure, but that it may be possible to distinguish between the active present-day hydrothermal system and an older and cooler part of the system. The densified region is compared spatially to self-potential, thermal and seismic results and we find a good concordance between the different geophysical data sets. Our results agree with previous studies that have indicated that the main feeder fault recharging the East Mesa reservoir dips steeply to the west.

Introduction

The origin of the East Mesa geothermal field is generally believed to be related to crustal extension, accompanied by normal faulting and possible dike injection, due to dextral offset between branches of the Imperial and Brawley faults (Hill et al., 1975; Hill, 1977; Weaver and Hill, 1979). On the basis of hypocenter locations, focal mechanisms, and fault scarps (Sharp, 1976), Hill (1977) proposed a tectonic model for the Brawley area, shown in Fig. 1. However, the East Mesa thermal anomaly remains something of an enigma in the tectonic framework of the Imperial Valley. In recent years it has beeen seismically quiet (Majer et al., 1978) and the structure and tectonics are not as well understood as they are for the recently active region near Brawley (Fuis et al., 1982).

More than a dozen geothermal development holes have been drilled on the East Mesa thermal anomaly. Neither basement rocks nor igneous intrusives have been thus far identified in any of the wells. There is growing evidence that the geothermal reservoir is a fault-charged system tapping a large primary reservoir of hot fluids at depth (Riney et al., 1979; Goyal and Kassoy, 1981).

In this paper we carefully analyze the residual Bouguer gravity anomaly by means of an inversion technique, and attempt to relate the anomaly to hydrothermal densification of rocks caused by heated water ascending along near-vertical fault zones.

The Reservoir Model

Goyal and Kassoy (1981) developed a conceptual reservoir model for the system on the basis of existing geological, geophysical and temperature data and supported by numerical modeling. They concluded that the system appears to be fault charged with thermal waters (~200 °C) rising along a system of near-vertical conduits 100 to 300 m wide. The water flow is essentially isothermal until the fluids reach a cooler, impermeable caprock at which point the fluids flow laterally into a thick aquifer, of constant permeability, losing heat to the caprock. Goyal and Kassoy's calculated maximum steady-state heat flux of 7.5 HFU (1 HFU = 1 $\mu cal/cm^2 \cdot s \sim 41.8\ mW/m^2$) matched the observed data, but the measured heat flux profiles are considerably different suggesting that the real system is more complex than the model proposed by these authors.

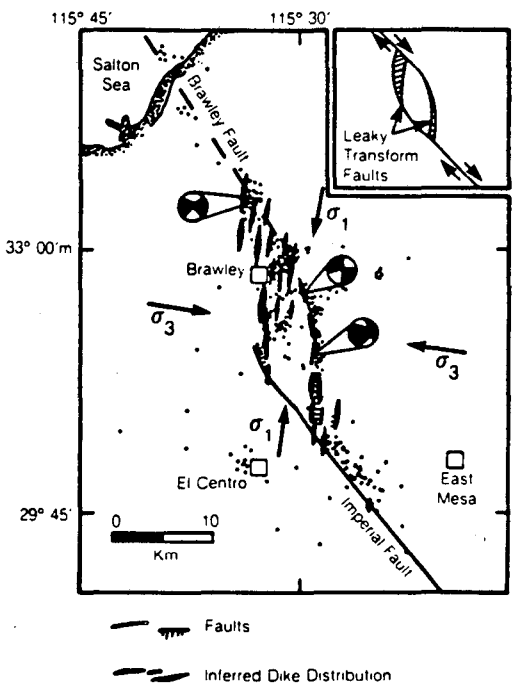

Fig. 1. Map of the Imperial Valley showing earthquake epicenters (dots) for swarms in June 1973. Hachures indicate normal faulting based on fault scarps (Sharp, 1976). The figure is after Hill (1977) and Weaver and Hill (1979). XBL 865-10800

Hoagland (1976) carefully studied drill cuttings from well 6-2, drilled to a depth of 1830 m near the center of the heat flow anomaly. He found that a thick section of clay-rich sediments grades downward into sandier units typical of basin margin facies and Colorado River delta sands deposited in an alluvial/lacustrine environment. Shown in Fig. 2 is a temperature profile from well 6-2, modified from Hoagland (1976), taken after a three-week shut-in period. Also shown is the depth range of some of the major authigenic (post-depositional) minerals observed. At a depth of about 900 m silicate-sulfide hydrothermal mineralization appears, and the transition to quartz, pyrite, illite, chlorite, and chert is regarded to mark the top of the reservoir. All these secondary minerals occur as pore-fillings and as replacements of detrital minerals. Quartz is the main authigenic mineral, and extensively quartz-cemented rocks are common below 930 m. Hoagland (1976) found evidence for at least three distinct episodes of silica precipitation, and also noted some dissolution of the original carbonates and micas in the zone of silicate-sulfide alteration. On the basis of the γ-γ density log, Hoagland reported that cementation and alteration gradually increase the average rock density from around 1.9 g/cm^3 at 670 m to 2.2 to 2.3 g/cm^3 below 914 m. It is commonly believed that hydrothermal densification of the sediments is the principal cause of the residual Bouguer gravity high over the field (Biehler, 1971).

To examine in more detail the morphology of the densified zone and to examine the conceptual model of a fault-charged reservoir, we carried out a 3-D inversion of the residual Bouguer gravity anomaly. In the next section we outline the inversion method and discuss the results.

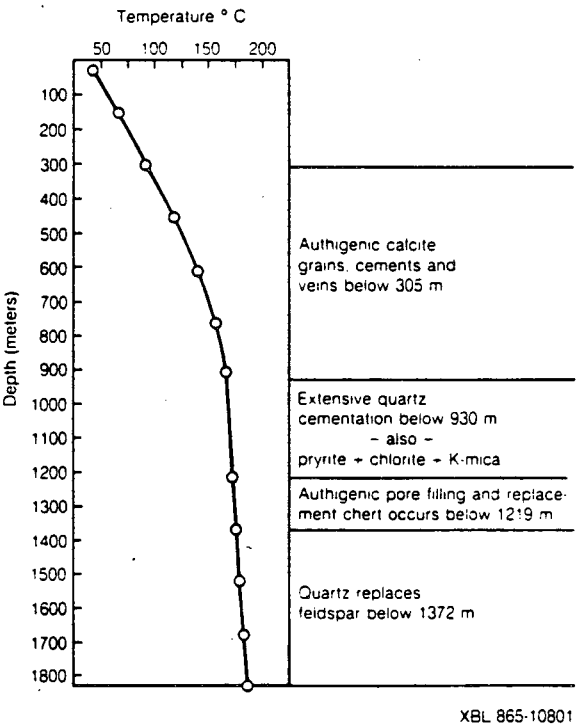

Fig. 2. Temperature profile in well 6-2 after three weeks of shut-in. Also shown are the depth and types of secondary hydrothermal minerals that occur as pore-fillings and replacements of detrital minerals (Hoagland, 1976).

Gravity Interpretation

Our model for the hydrothermal densification associated with the geothermal field is shown schematically in Fig. 3. The normal density section for the southeast corner of the Imperial Valley is based on seismic velocities (Fuis et al.,

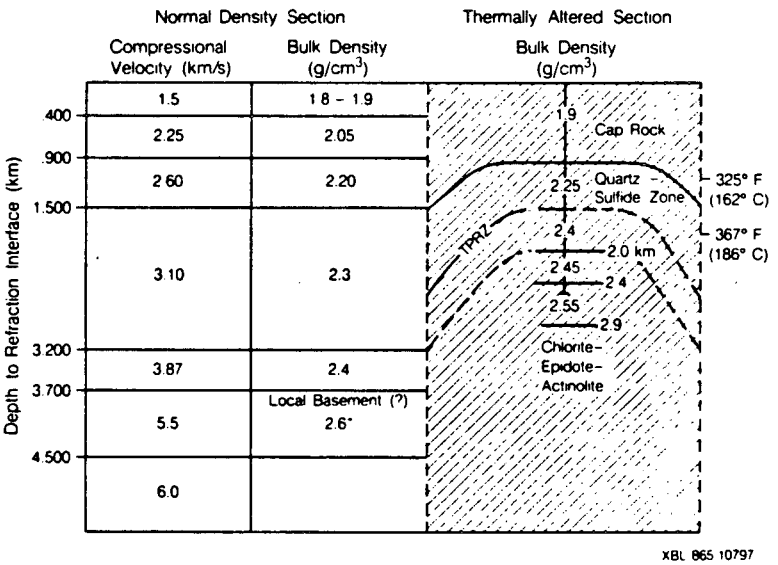

Fig. 3. A comparison of bulk densities for both unaltered and thermally altered sections. The unaltered densities are based on seismic velocities (Fuis et al., 1981). The densities within the East Mesa geothermal field are based on geophysical log data. TPRZ is the approximate configuration for the top of the poorly reflective zone (van de Kamp et al., 1978). There is no drill hole evidence reported yet for a high temperature chlorite-epidote-actinolite zone.

1981), and those densities are shown on the left of the figure. For a point directly over the thermal and gravity anomalies the densities of the thermally altered rocks are based on the average bulk density from γ-γ density logs. Notice that densities increase with depth in both sections, but below the caprock the density of the hydrothermally altered section is about 0.1 to 0.2 g/cm^3 greater than that of the normal section at a comparable depth. TPRZ denotes the top of the poorly reflective zone identified by van de Kamp et al. (1978) as the point below which coherent seismic reflections are lost. Directly over the thermal anomaly the TPRZ occurs at a depth of 1500 to 1700 m. There is not yet evidence for it, but we show in Fig. 3 the possibility of a deeper, central core of higher temperature hydrothermal minerals where temperatures may have exceeded 250°C for some protracted period in the past.

Because it appears that the density contrast between the altered and unaltered section below the caprock is invariant with depth, we can model the residual anomaly (Fig. 4) as an excess mass consisting of a bundle of square prisms of variable height above a reference depth, assumed to be the basement depth of 3.7 km (Fig. 5). The density difference, $\Delta\rho$, between the prisms and the host medium may be specified if that information is available, but in the problem here we will solve explicitly for $\Delta\rho$.

To solve the thickness T_q of each prism and the contrast $\Delta\rho$ we use an iterative 3-D inversion procedure based on the approach described by Cordell and Henderson (1968). The residual gravity anomaly in an area of 9.5×10 miles was digitized on a square grid at a station spacing of 0.5 mile. Centers of the vertical prisms coincide with the grid points (Fig. 5). By specifying values for $\Delta\rho$ and the depth, D, to the reference plane, the gravity effect of the entire bundle of M prisms at the p-th grid point is:

$$g_p \approx \gamma \sum_{q=1}^{M} f(P, Q, T_q; \Delta\rho_1, D), \qquad (1)$$

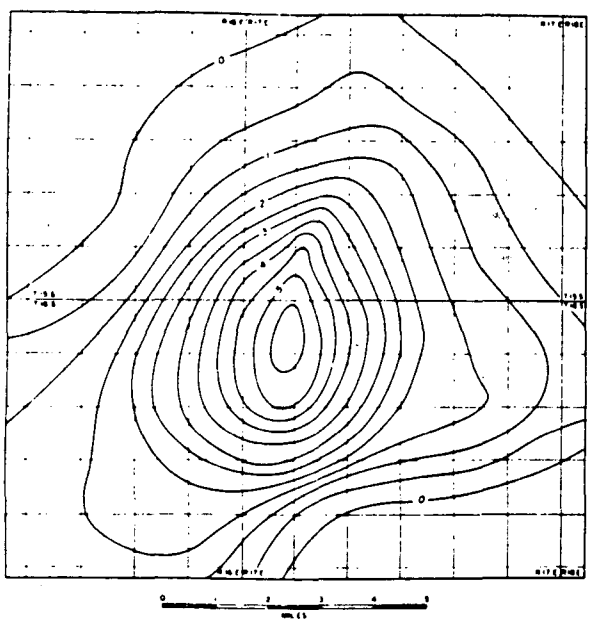

XBL 7810-11720

Fig. 4. Residual Bouguer gravity anomaly of the East Mesa area (Biehler, 1971). Contour interval is 0.5 mGal.

where

P is the p-th grid point P: (x, y, 0),

Q is the q-th prism centered at Q: (x′ , y′ , 0),

γ is the gravitational constant,

T_q is the height of the q-th prism, and

$\Delta\rho_1$ is the initial value of $\Delta\rho$.

Whereas Cordell and Henderson (1968) formulated their procedure on the assumption that prisms heights go to zero in all perimeter blocks around the grid, this is generally not a safe assumption. For this reason we treat each perimeter block as a slab of non-zero thickness extending to infinity in one direction; the four corner blocks are treated as quarter-space slabs extended to infinity in two directions.

Following the approach of Cordell and Henderson (1968), we used an iterative procedure such that if $t_{n,q}$ is the height of the prism q at the n-th iteration, then

$$\lim_{n\to\infty} t_{n,q} = T_q, \text{ for all q.}$$

The initial guess $t_{1,q}$ is obtained by using the Bouguer slab formula:

$$T_{1,q} = g_{obs,q}/2\pi\gamma\Delta\rho_1.$$

Using these heights and the appropriate expressions for the gravitational attraction of a finite vertical prism, we calculate the anomalous gravity for each grid point, $g_{calc,1,q}$. Next, we adjust the height of the prisms for the second iteration as follows:

$$t_{2,q} = t_{1,q}\left(\frac{g_{obs,q}}{g_{calc,1,q}}\right). \qquad (2)$$

For subsequent iterations Eq. 2 can be written in a generalized form as

$$t_{n+1,q} = t_{n,q}\left(\frac{g_{obs,q}}{g_{calc,n,q}}\right).$$

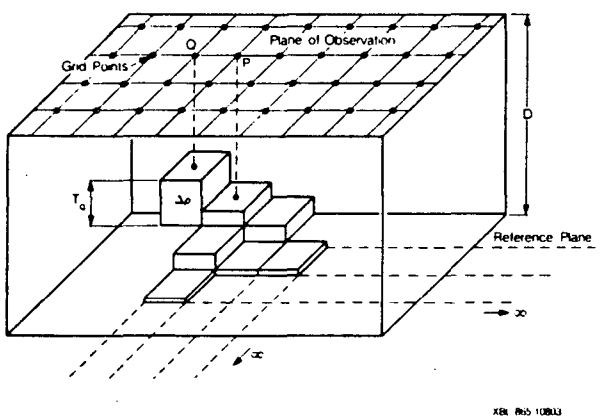

Fig. 5. Representation of the densified zone as a bundle of square prisms of variable and unknown height above a reference plane, assumed to be the basement depth of 3.7 km. The prisms have a constant but unknown density contrast, $\Delta\rho$, with respect to the host rocks.

After several iterations, usually four, we stop and adjust $\Delta\rho$, by introducing the constraints that one or more prism heights may be known from geophysical well logs, cores, and/or cuttings. In the East Mesa problem we used the depth to the densified zone in well 6-2 (Hoagland, 1976) to solve for the adjusted density contrast, $\Delta\rho_2$,

$$\Delta\rho_2 = \Delta\rho_1 \frac{t_{m,q}}{T_q}, \qquad (3)$$

where $t_{m,q}$ is the calculated height of the prism at the well location after m iterations and T_q is the height of that prism from the drill hole data. Prism thicknesses are again iterated using $\Delta\rho_2$ and the whole procedure is repeated several times. It was found after six density values or a total of 24 prism iterations every calculated gravity value was within the precision of the corresponding residual anomaly value; i.e., the two values converge to within 0.1 mGal at every grid point.

If the top of the densified zone has been determined by more than one drill hole, then each adjusted value of $\Delta\rho$ would be an averaged value over the K holes:

$$\Delta\rho_{i+1} = \frac{\Delta\rho_i}{K} \sum_{k=1}^{K} \frac{t_{m,k}}{T_k}.$$

There are several sources of error in this interpretative approach which limit the accuracy of the densified zone model away from the drill holes. These include (a) the accuracy of the residual anomaly, (b) the choice of the reference depth, and (c) departure from an invariant density contrast. However, all gravity interpretations, regardless of the method used, are limited by errors in the data set or by errors that are introduced by assumptions about the source body.

The Gravity Results

Figures 6 and 7 show the depth (in meters) to the density interface for calculations using gridded data at one-mile and 0.5-mile separations, respectively. The one-mile grid gives a station density close to the actual average gravity station density in the area. The 0.5-mile separation was considered for the purpose of comparing resolutions, and because it appeared that the residual anomaly was sufficiently smooth to be modeled at the higher data density without introducing serious errors. Both models show a dominant north-south-trending densified zone whose northern end curves and deepens to the northeast. A small parasitic zone, seemingly disconnected from the main zone, lies to the southeast. Not surprisingly, the lower resolution data set produces a slightly broader (overall) zone, and a corresponding slightly lower (~20%) density contrast. The higher resolution data set produces a sharper north-south feature. It appears to be intersected by at least one northwest-trending density structure which we believe is genuine, not an artifact of the numerical procedures.

Comparison of the Density Model to Other Geophysical Results

To obtain a sense for the validity and significance of the 3-D gravity inversion results, we next compared the density anomaly to other geophysical data; namely, the trends of possible faults reported on the basis of seismic monitoring, reflection seismic interpretations, self-potential anomalies,

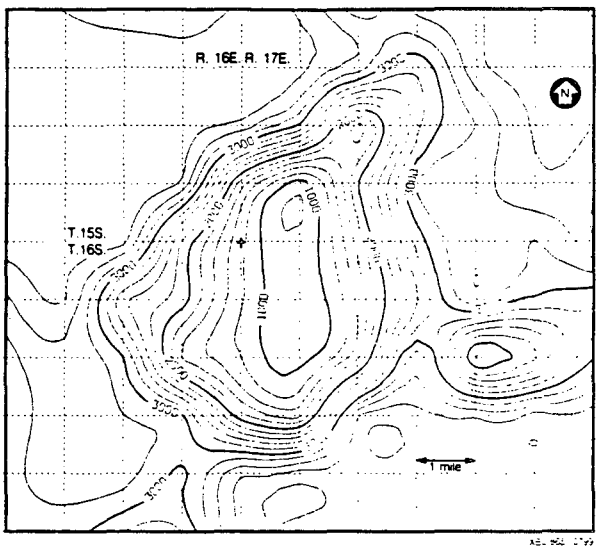

Fig. 6. Depth (meters) to the top of the densified zone using gridded data at a one-mile separation. $\Delta\rho = 0.11$ g/cm^3.

and temperature data. Figure 8 shows the relation of the subsurface temperature contours at a depth of 1200 m (G.R. Zebal, pers. comm., 1984) to the densified zone. Although the isotherms are not too well constrained by subsurface temperature data, there is a reasonably good general correlation between temperature and density. Three main features stand out:

1. The parasitic density anomaly to the southeast, and the northern end of the main anomaly are both in areas of declining temperatures. If real, both densified zones

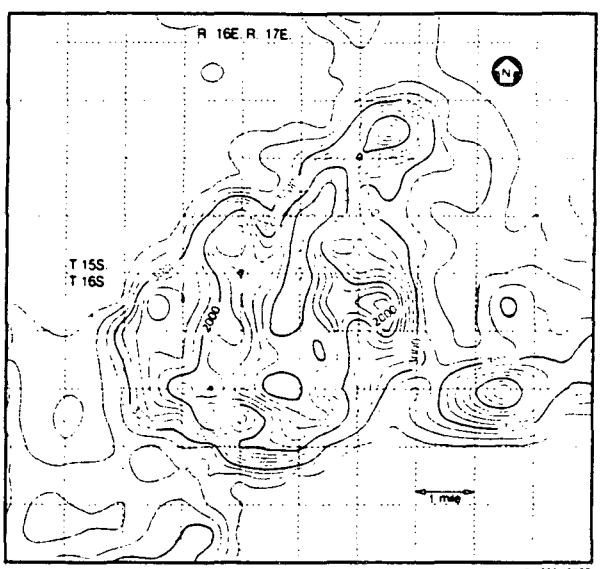

Fig. 7. Depth (meters) to the top of the densified zone using gridded data at a half-mile separation. $\Delta\rho = 0.14$ g/cm^3.

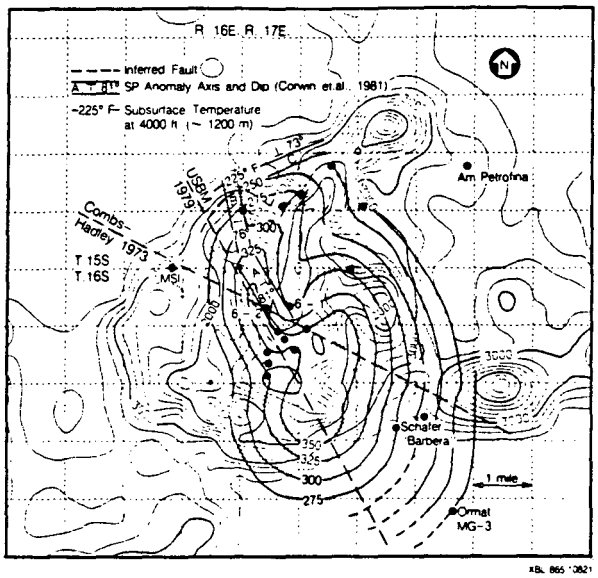

Fig. 8. Comparison of the contours on the top of the densified zone (Fig. 7) to temperatures at 1200 m, inferred faults, and self-potential anomalies. The solid circles are wells.

may correspond to older, deeper and cooler segments of the hydrothermal system.

2. The double lobe seen on the northern end of the temperature anomaly is related to density features resolved only in the analysis of the higher station density gravity data set. The more pronounced of these lobes, the northwest one, also correlates very closely with the axis of a dipolar self-potential anomaly (A) and another SP trend (B) as interpreted by Corwin et al. (1981).

3. The zones of maximum temperature do not coincide exactly with the zones of shallowest depth to the densified zone. The two features are slightly displaced. This may be a result of a fortuitous condition that prevents the feeder zones from self-sealing or it may indicate a dipping feeder fault.

To compare further the density anomaly and the heat flow anomaly, we made a check calculation on the assumptions that the main feeder conduit (like the densified zone) can be approximated by an isothermal, 2-D dike of large depth extent, and that steady-state thermal conditions exist. For a zone at a depth of 915 m (the approximate caprock thickness) and with a half-width of 300 m (Corwin et al., 1981; Goyal and Kassoy, 1981), we solved for the zone temperature needed to cause the heat flow anomaly of 6.35 $\mu cal/cm^2 \cdot s$ above background. The estimated temperature using the method of Horai (1976) is 179 °C (355 °F), a value in close agreement with the measured maximum temperatures.

There does not seem to be any convincing correlations between microseismic activity and the densified zones. For completeness we show two fault trends reported in the literature. Combs and Hadley (1977) identified a right-lateral strike-slip fault (Mesa fault) on the basis of 36 locatable earthquakes with epicenters in an elliptical area over the thermal anomaly. The fault labeled USBM 1979, taken from U.S. Bureau of Reclamation (1979), is an inferred fault aligned with the trend of the surface heat flow anomaly.

We do not show it in Fig. 8 because it would overly complicate the map, but van de Kamp et al. (1978) found evidence for faults in the reflection seismic data that closely match the trend and location of the northwest temperature-density lobe and the SP anomaly axis (A). Figure 9 is an east-west cross-section through wells 6-2 and 6-1. The section, after van de Kamp et al. (1978), shows the relationships between the top of the densified zone (TDZ), the 350 °F (177 °C) and 375 °F (190 °C) isotherms and faults and other features observed in the seismic section. Notice that the displaced thermal and density anomalies agree in location with the position of a fault dipping steeply to the west.

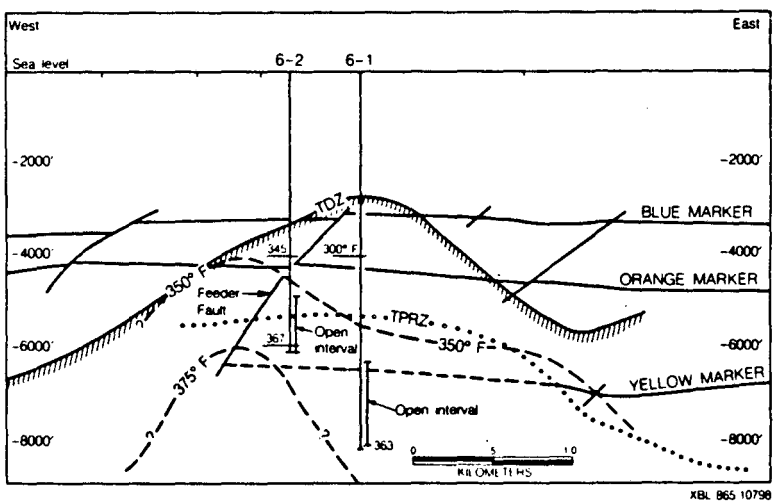

Fig. 9. East-west cross section through well 6-2 and 6-1, showing faults and reflecting horizons (van de Kamp et al., 1978), the 350 °F and 375 °F isotherms, and the top of the densified zone (TDZ). The shape of the isotherms relative to the TDZ suggest that hydrothermal fluids rise along a fault zone that dips steeply to the west, denoted as the feeder fault.

Conclusions

A 3-D inversion of the gravity data, constrained by information from drill hole logs and a petrographic-alteration study, provides further evidence that the reservoir rocks of the East Mesa geothermal field are being fed by thermal waters ascending along a complex set of faults. The precipitation of a denser suite of authigenic silicate-sulfide minerals along the feeder zones and laterally outward into permeable horizons below a caprock, explain the density contrast and the resulting residual Bouguer anomaly. The fact that the axes of the densified zones are slightly displaced laterally from the subsurface temperature maxima suggests that the feeder zones could be dipping in a direction toward the temperature maxima. A feeder zone dipping steeply to the west agrees with the seismic reflection cross-section and with the SP interpretation.

When studied along with other geophysical information the gravity inversion results indicate that the reservoir has been fed by a complex set of faults, segments of which are in older and presently cooler parts of the hydrothermal system. Whereas the principal part of the density anomaly runs in an north-south direction, curving to the northeast at its northern end, the present-day hydrothermal activity seems to be associated with a northwest-trending lobe. This lobe of the density anomaly also correlates with temperature and SP anomalies and with faults inferred from seismic reflection surveys.

To resolve the density features, we recommend that gravity stations over the main parts of the anomalies be located no more than 0.5 miles apart.

Acknowledgements

This work was supported by the Assistant Secretary for Conservation and Renewable Technology, Office of Renewable Energy Technologies, Geothermal Technology Division of the U.S. Department of Energy under Contract No. DE-AC03-76SF00098. The authors would like to thank Tom Hinrichs, President of Imperial Magma, and Walt Haenggi and Fred Teeters of the parent company, Dow Chemical USA, for helpful discussions.

References

Biehler, S., 1971, Gravity studies in the Imperial Valley *in* Rex, R.W., et al., eds., Cooperative geological-geophysical-geochemical investigations of geothermal resources in the Imperial Valley of California: Univ. of Calif., Riverside, p. 29-41.

Combs, J., and Hadley, O., 1977, Microearthquake investigations of the Mesa geothermal anomaly, Imperial Valley, California: *Geophysics*, v. 42, p. 17-33.

Cordell, L., and Henderson, R.G., 1968, Iterative three-dimensional solution of gravity anomaly data using a digital computer: *Geophysics*, v. 33, n. 4, p. 596-601.

Corwin, R.F., De Moully, G.T., Harding, R.S., Jr., and Morrison, H.F., 1981, Interpretation of self-potential results from the East Mesa geothermal field: *J. Geophys. Res.*, v. 86, p. 1841-1848.

Fuis, G.S., Mooney, W.D., Healey, J.H., McMechan, G.A., and Lutter, W.J., 1981, Seismic refraction studies of the Imperial Valley region, California–profile models, a traveltime contour map, and a gravity model: U.S. Geol. Survey *Open-File Report 81-270*, 73 p.

_____, 1982, Crustal structure of the Imperial Valley region *in* The Imperial Valley, California, Earthquake of October 15, 1979: U.S. Geol. Survey, *Prof. Paper 1254*, p. 25-49.

Goyal, K.P., and Kassoy, D.R., 1981, A plausible two-dimensional vertical model of the East Mesa geothermal field, California: *J. Geophys. Res.*, v. 86, n. B11, p. 10719-10733.

Hill, D.P., 1977, A model for earthquake swarms: *J. Geophys. Res.*, v. 82, n. 8, p. 1347-1352.

Hill, D.P., Mowinkel, P., and Peak, L.G., 1975, Earthquakes, active faults and geothermal areas in the Imperial Valley, California: *Science*, v. 188, n. 4195, p. 1306-1308.

Hoagland, J.R., 1976, Petrology and geochemistry of hydrothermal alteration in borehole Mesa 6-2, East Mesa geothermal area, Imperial Valley, California: M.S. thesis, Department of Earth Sciences and Inst. Geophys. and Planet. Phys., Univ. Calif. Riverside, *IGPP-UCR-76-12*, 90 p.

Horai, K., 1976, Heat flow anomaly associated with dike intrusion, 2: *J. Geophys. Res.*, v. 81, n. 5, p. 894-898.

Majer, E.L., McEvilly, T.V., Schechter, B., and Goldstein, N.E., 1978, Section 2: Seismicity *in* Geothermal resource and reservoir investigations of U.S. Bureau of Reclamation leaseholds at East Mesa, Imperial Valley, California: Lawrence Berkeley Laboratory, *LBL-7094*, p. 33-55.

Riney, T.D., Pritchett, J.W., Rice, L.F., and Gary, S.K., 1979, A preliminary model of the East Mesa hydrothermal system: *Proc. Fifth Annual Workshop on Geoth. Reserv. Eng., Stanford University, SGP-TR-40*, p. 211-214.

Sharp, R.V., 1976, Surface rupturing in Imperial Valley during the earthquake swarm of January–February 1976: *Bull. Seism. Soc. Am.*, v. 66, p. 1145-1154.

U.S. Bureau of Reclamation, 1979, Geothermal resource investigations, East Mesa test site, Imperial Valley, California: Concluding Report.

van de Kamp, P.C., Howard, J.H., and Graf, A.N., 1978, Section 1: Geology *in* Geothermal resources and reservoir investigations of U.S. Bureau of Reclamation leaseholds at East Mesa, Imperial Valley, California: Lawrence Berkeley Laboratory, *LBL-7094*, p. 1-32.

Weaver, C.S., and Hill, D.P., 1979, Earthquake swarms and local spreading along major strike-slip faults in California *in* Rybach, L., and Stegena, L., eds., Geothermics and Geothermal Energy, Contributions to Current Research in Geophysics (CCRG): Birkhäuser Verlag, Basel, p. 55-64.

LAWRENCE BERKELEY LABORATORY
TECHNICAL INFORMATION DEPARTMENT
UNIVERSITY OF CALIFORNIA
BERKELEY, CALIFORNIA 94720